Carbon 122 (2017) 446–450

Contents lists available at ScienceDirect

Carbon

journal homepage: www.elsevier.com/locate/carbon

Adhesionless and near-ideal contact behavior of graphene on Cu thin film

M. Hammad [a, b], J.-J. Adjizian [c], C.-H. Sacré [a], B. Huet [b], J.-C. Charlier [c], J.-P. Raskin [b], T. Pardoen [a, *]

[a] Institute of Mechanics, Materials and Civil Engineering (iMMC), Université Catholique de Louvain, B-1348, Louvain-la-Neuve, Belgium
[b] Information and Communication Technologies, Electronics and Applied Mathematics (ICTEAM), Université Catholique de Louvain, B-1348, Louvain-la-Neuve, Belgium
[c] Institute of Condensed Matter and Nanosciences (IMCN), Université Catholique de Louvain, B-1348, Louvain-la-Neuve, Belgium

ARTICLE INFO

Article history:
Received 6 April 2017
Received in revised form
11 June 2017
Accepted 14 June 2017
Available online 16 June 2017

ABSTRACT

Graphene coatings reduce surface adhesion owing to a low surface energy. In the present work, a single CVD-grown graphene layer on Cu is shown to modify the elastic contact behavior by eliminating adhesion. Nanoindentation load-displacement curves exhibit higher load bearing capacity for Cu/graphene in the elastic regime compared to bare Cu and a closer agreement with Hertz law. Molecular dynamics simulations confirm the quasi-absence of adhesion between graphene and indentor tip. These results open new opportunities regarding tribological issues related to coatings or MEMS applications.

1. Introduction

Graphene [1] exhibits a panoply of outstanding properties being atomically thin, transparent [2], impermeable [3] and one of the strongest materials ever [4]. Graphene coatings have shown significantly enhanced protection against diffusion and oxidation [5] as well as improved wear durability [6], and enhanced thermal conductivity [7]. Moreover, graphene has a low surface energy as measured by liquid contact angle [8], while pull-off force measurements have clearly demonstrated that the presence of graphene could reduce surface adhesion [9]. Atomistic simulations of nanoindentation on graphene coated platinum shows higher load bearing capacity than bare platinum surfaces within the elastic regime [10], while atomic force microscopy sub-nanometer indentation exhibits an excellent agreement for epitaxial graphene between experimental elastic load-displacement curves and the Hertz model [11]. However, to our knowledge, the complete understanding of the effect of the presence of a graphene layer on the elastic response of metallic surfaces to nanoscale contact has not been extensively studied. Given the importance of surface adhesion and the contact behavior of graphene coated surfaces to many applications, a better insight into graphene's adhesion and contact properties is required. In this work, we show that a single layer of chemical vapor deposition (CVD) grown graphene transforms the Cu surface into a near ideal adhesionless contact surface when subject to nanoindentation, leading to a higher load bearing capacity as well as a near ideal Hertzian contact behavior. This quasi-absence of adhesion in the Cu/graphene system is demonstrated by performing nanoindentation within the elastic penetration regime, further rationalized by both Finite Elements (FE) and Molecular Dynamics (MD) simulations. Aside from fundamental interest, this adhesion-less property could be advantageously used for instance in MEMS applications where contact and material transfer is an issue, e.g. RF switches [12–14].

2. Experimental

Two samples were prepared by evaporating a thin Cu layer on a Si wafer with a 300 nm wet oxide. The Cu film thickness is ~750 nm. The first sample was covered by graphene using chemical vapor deposition (CVD) [15] with Ar/H_2 and Ar/CH_4 gas mixture (see experimental details in supplementary material); the other sample was exposed to Ar/H_2 only while undergoing the same heat treatment with the same temperature profile. SEM imaging (Fig. 1a) and Raman spectra (Fig. 1b) confirmed that the grown graphene is a single layer with almost no defects (Note the absence of D peak in Fig. 1b and in the original spectrum in supplementary material). Nanoindentation experiments were performed with an Agilent

* Corresponding author.
E-mail address: thomas.pardoen@uclouvain.be (T. Pardoen).

http://dx.doi.org/10.1016/j.carbon.2017.06.037
0008-6223/

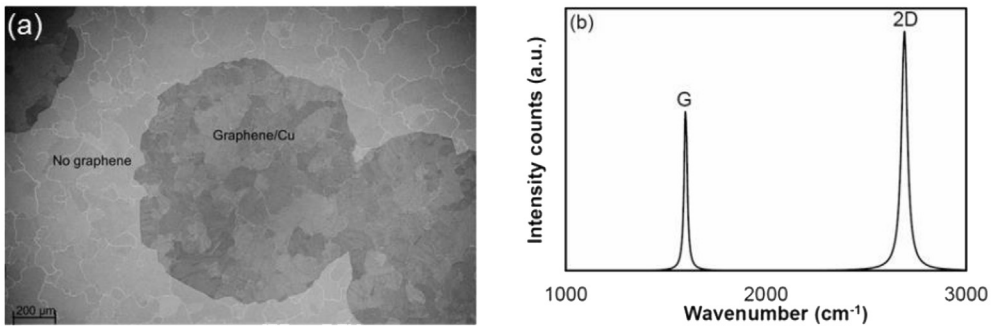

Fig. 1. (a) SEM image and (b) fitted Lorentzian peaks of the Raman spectrum of CVD grown graphene on Cu thin film.

nanoindenter utilizing the continuous stiffness measurement (CSM) method using a diamond Berkovich tip with a diameter of the rounded extremity of ~40 nm. 120 indents were performed under displacement controlled mode on each sample in order to generate statistically robust results.

As long as the indentation depth is shallow enough, the contact between the indenter and the surface is purely elastic. The end of the elastic regime appears with a first "pop-in" indicating the first plastic burst, typically at an indentation depth between 8 and 12 nm for Cu [16]. At the initial shallow indentation depth, the mechanics of the contact is dictated by the rounded shape of the tip, assimilated here as a sphere with 20 nm radius. Ideally, the response should follow the Hertz law of contact which is the ideal scenario between two isotropic elastic bodies in the limit of small strain conditions [17]. The Hertz law expresses the relationship between load and displacement in the form $P = kh^n$, where P is the load, k is a constant, and h is the displacement and n is equal to 1.5. Most often, experimental results do not perfectly match with Hertz model due to several factors: surface anisotropy, friction, and adhesion between the surface and the tip. Often, the indenter tip is not perfectly spherical. Nevertheless, early experimental and simulation works on nanoindentation of tungsten have shown that even irregular shaped tips result in load-displacement relationships that could be perceived as originating from a spherical tip, but with a slight deviation [18], which further validates the idea of comparing our results to Hertz law.

Fig. 2a displays the initial elastic part of the load-displacement curve for both Cu and Cu/graphene surfaces. The curves represent an average of the 120 single indents (examples of single indentation curves are shown in supplementary material). The Cu/graphene surface exhibits an initial stiffer response and withstands higher loads than bare Cu at the same indentation depth; similar to what has been suggested by simulations of Pt/graphene and bare Pt surfaces [10]. Moreover, by fitting the curves with Hertz relationship $P = kh^n$, one finds $n = 2.1$ for Cu and $n = 1.42$ for Cu/graphene, indicating that the Cu/graphene system leads to indentation response closer to Hertz theoretical prediction. These results demonstrate that graphene drastically modifies the elastic contact between Cu and the tip for penetration depths much larger than 10 times the graphene layer thickness. In order to understand the specific impact that graphene induces on the contact response, a few possible causes have been considered and investigated:

1. The high stiffness of graphene;
2. The difference of friction between the tip and bare Cu versus between the tip and Cu/graphene;
3. The difference of adhesion between the tip and bare Cu versus between the tip and Cu/graphene.

3. Simulations

In order to assess the first hypothesis, FE simulations have been performed to investigate the effect of the high graphene stiffness on the nanoindentation load-displacement curve. Graphene Young's modulus has been predicted and measured in many previous studies [4,19,20] and the estimated value is ~1 TPa. On the other hand, the Young's modulus of Cu is measured to be around 100 GPa from the load-displacement curves of bare Cu (see supplementary material). An axisymmetric FE model was created using a rigid spherical tip with a radius R indenting with a displacement U and exerting a load P on a system consisting of two materials (See supplementary material for details): an ultrathin film (thickness $= t_f$) with Poisson ratio ν_f equal to 0.2 and a Young's

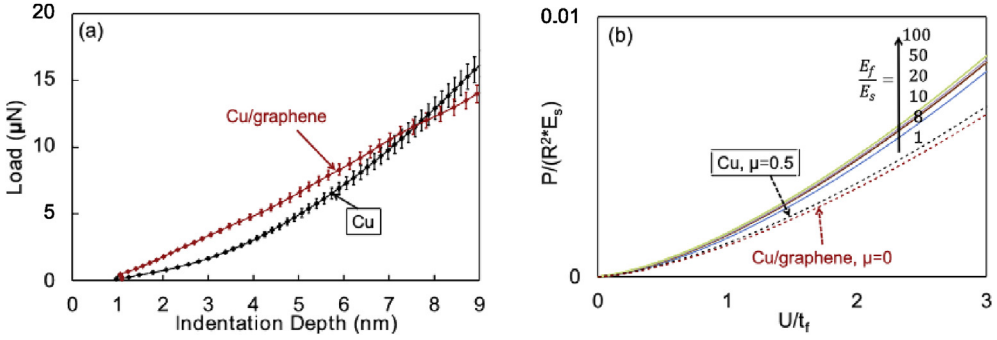

Fig. 2. Load-displacement curves: (a) experimental measurements for Cu and Cu/graphene, theoretical modelling using a FE approach (b) for different film/substrate moduli ratio (solid lines) and for different friction coefficients between the tip and the surface (dotted lines). Dimensionless load vs dimensionless displacements are plotted in (b). All symbols are defined in the text. (A colour version of this figure can be viewed online.)

modulus E_f on a substrate with a Young's modulus E_s taken equal to 100 GPa, and with a thickness t_s and a Poisson ratio ν_s equal to 0.34. In order to investigate the effect of the film stiffness on the elastic contact behavior, the ratio of E_f/E_s was varied from 1 to 100. In the case of Cu/graphene, the E_f/E_s ratio is expected to be around 10. However, due to the extremely small thickness of graphene, its high stiffness affects the load-displacement curve only for penetration depths on the order of the film thickness as illustrated in Fig. 2b (solid lines). Consequently, the high stiffness of graphene and the film/substrate moduli ratio cannot explain the experimental results shown in Fig. 2a.

It has also been shown that graphene can act as a solid lubricant, reducing the friction between the coated surface and other surfaces [9,21,22]. In order to test the effect of friction between the tip and the indented surface, the FE model described above has been used again. In this simulation, we assume that in the presence of graphene, the contact between the tip and the surface is frictionless with a friction coefficient $\mu = 0$ and that in the absence of graphene, the friction coefficient μ is equal to 0.5. The predicted load-displacement curves (dotted lines in Fig. 2b) suggest that changing the friction between the tip and the surface does not result in any significant change in the apparent indentation stiffness. As a matter of fact, a lower friction coefficient leads to an apparently slightly softer response which is opposite to the experimental measurements (Fig. 2a).

Consequently, the only remaining option to explain the results of Fig. 2a is to invoke the possible impact of the interaction forces between the tip and the indented surface. It is presumed that an adhesionless contact will induce higher load responses for the same displacement. Indeed, in the presence of an adhesion force, the load required to achieve a certain displacement is partly provided by this adhesion force. When the adhesion force is absent, the tip must exert the entire load required to achieve the same displacement. In order to validate this assumption, MD simulations have been performed using the LAMMPS code [23]. A rigid fullerene-like tip with a 30 nm diameter is placed 2 Å above a single graphene layer on a Cu (111) substrate (Fig. 3a). It is expected that there should be a difference between the experimental tip diameter and the corresponding theoretical value used in the simulation. This can be justified by the fact that the nanoindenter tip is rough and hard; anomalies in diameter are expected especially at shallow indentation depths. Therefore, additional MD simulations have been performed with a 6 nm diameter tip, which shows closer agreement with the experimental results in terms of load values. In this model, the copper film is characterized by a length of 100 nm, a width of 100 nm, and a thickness of 7 nm. Periodic boundaries are used in the planar (x and y) atomic directions in order to avoid any edge effect (see supplementary material for details). This theoretical model tries to mimic as close as possible the experimental setup. The choice of the interatomic potentials is crucial, especially to accurately model the forces between Cu and C atoms. Previous theoretical studies with different classical potentials have been reported in literature [24–31] to model the interaction of C and Cu during nanoindentation, nanoscratching and nanofriction experiments. In the present study, the Tersoff potential for C atoms [32], the embedded atom model (EAM) potential for Cu atoms [33] and a Morse potential for Cu-C interaction ($D = 0.1$ eV, $\alpha = 1.7$ Å and $r_0 = 2.1$ Å) [34] were used. The bottom layer of the Cu slab remains fixed during the entire simulation, and the tip is initially fixed as well. A conjugate gradient algorithm, as implemented in LAMMPS, is used for energy minimization. The forces on all C atoms from the tip are recorded and summed up to calculate the overall load. Then, the tip is moved down by steps of 0.125 Å and the procedure is repeated until the tip has penetrated the surface by 1 nm.

Fig. 3b presents the load displacement curves extracted from the MD simulations for a 30 nm diameter tip and Fig. 3c shows the load-displacement curves for a 6 nm diameter tip. A fit is applied to both experimental and theoretical data using a polynomial function of type ax^b. Table 1 provides the values of parameters a and b resulting from the fits, showing a relatively good agreement

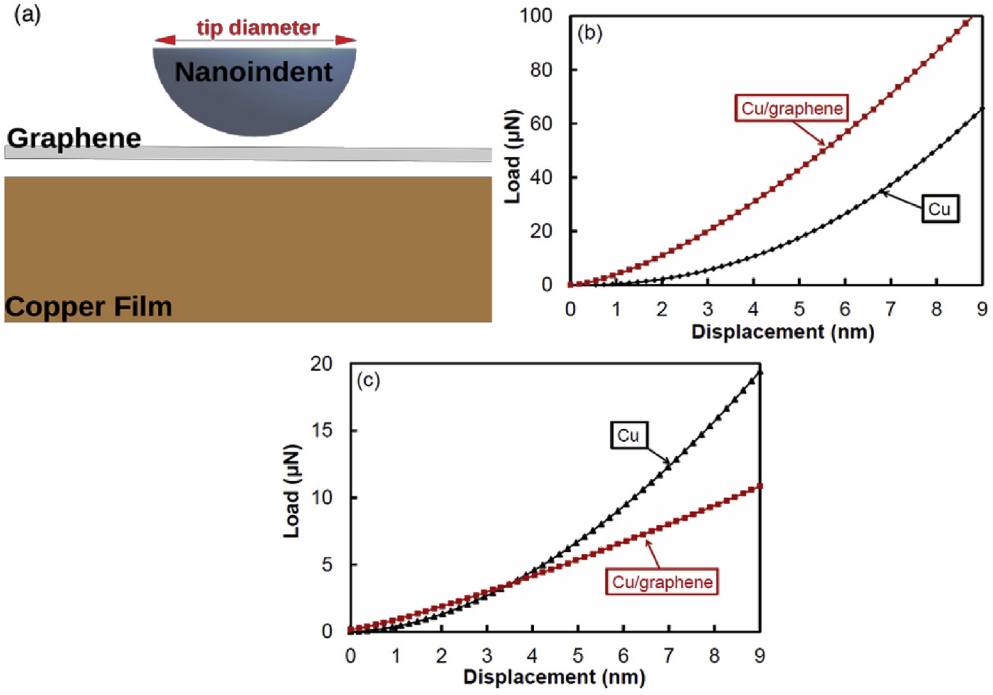

Fig. 3. (a) Schematic representation of nanoindentation in a Cu/graphene nanolayered composite with an ideal hemispherical carbon nanoindenter. MD simulations of load-displacement curves of a bare Cu (111) surface and a Cu (111) surface coated with graphene with (b) 30 nm diameter tip and (c) 6 nm diameter tip. (A colour version of this figure can be viewed online.)

Table 1
Parameters for the ax^b fit extracted from load-displacement curves obtained experimentally and theoretically for bare Cu and CVD grown graphene on Cu.

	Cu			Cu/graphene		
	Exp.	Theor. (30 nm)	Theor. (6 nm)	Exp.	Theor. (30 nm)	Theor. (6 nm)
a	0.166	0.47	0.377	0.68	3.8	0.735
b	2.1	2.24	1.8	1.42	1.49	1.39

between theory and experiment.

The MD simulations were analyzed in details in order to unravel the atomistic mechanisms related to the behaviors in both curves. In the case of bare Cu, Fig. 4a clearly shows that atoms are transferred to the tip during the contact which indicates adhesion between the tip and the surface. The presence of a single layer graphene completely eliminates this process as illustrated in Fig. 4b. Indeed, no atom is transferred from the surface to the tip and no adhesion is observed.

4. Discussion

Graphene was known to lower surface adhesion [9]. However, here, we show that graphene completely eliminates this atomic process, thus inducing an almost ideal contact behavior which follows Hertz law. MD simulations also suggest that when a larger tip (~30 nm) is indenting the surface, the effect is even more pronounced (see Fig. 3b and c). This aspect leads to additional points of discussion. In Ref. [9], graphene was transferred onto a SiO_2 surface. The graphene surface contained polymer residues from the transfer process which increased the surface energy. In our work, graphene is CVD-grown on the Cu surface, and is in its pristine state. Moreover, the adhesion between CVD-grown graphene and the underlying Cu film is larger than for transferred graphene, since during transfer, wrinkles and ripples may form, thus weakening the interaction between graphene and the substrate. Such a weaker interaction between graphene and the substrate allows the carbon layer to deform and conform around the tip increasing the contact area between them which leads to higher adhesion (see also recent analysis of friction behavior with similar findings [35]). On the contrary, a stronger interaction between graphene and the substrate prevents the deformation of the carbon layer and so keeps the adhesion minimized. This atomistic scenario also explains why the effect measured with a 30 nm tip is more pronounced than with a 6 nm tip, as a sharp tip will facilitate the bending and deformation of graphene around it. To confirm this hypothesis, additional nanoindentation experiments have been performed on transferred graphene onto both SiO_2 and Cu. These tests present an opposite effect for SiO_2/graphene (similar to what is observed in Ref. [36]), while graphene transferred on a Cu film shows a similar but weaker effect (see Fig. 5). It has been shown that adhesion between graphene and metals like Cu is almost 1.5 times larger than that between graphene and dielectrics like SiO_2 [37,38]. Therefore, even with graphene being similarly transferred on both surfaces, graphene on Cu is subject to lower adhesion with the indenting tip than graphene on SiO_2. It is worth noting that the difference in stiffness between both substrates is expected to play a role only in determining the contact behavior between the substrate with or without graphene coating and the indenting tip, but not on the effect of graphene modifying the surface interaction forces.

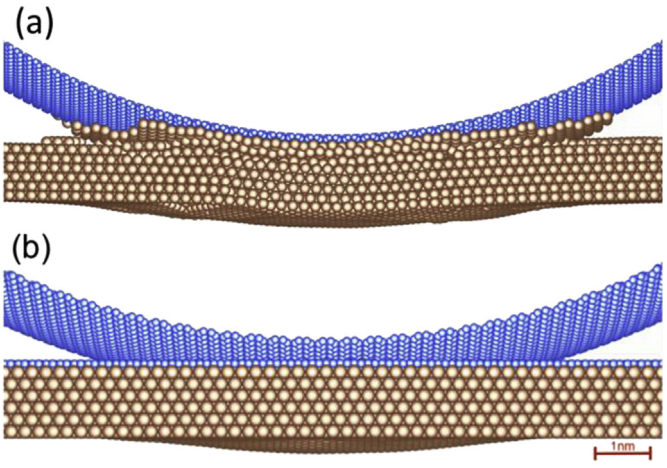

Fig. 4. Atomistic MD simulations of nanoindentation in (a) bare Cu and (b) Cu/graphene thin films. For a better visualization, a bigger tip (30 nm in diameter) is used to illustrate (a) the adhesion of Cu atoms to the nanoindenter tip and (b) the absence of transfer of Cu atoms (no adhesion) in the presence of a single layer of graphene. The scale bar is 1 nm. (A colour version of this figure can be viewed online.)

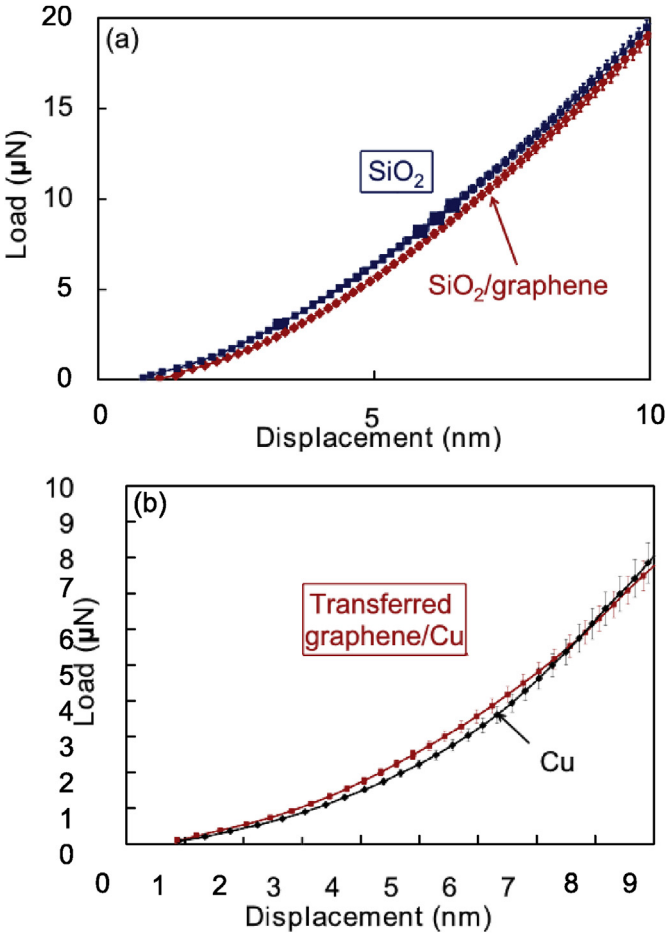

Fig. 5. Load-displacement curves: (a) experimental measurements for SiO_2 and SiO_2/graphene, and (b) experimental measurements for bare Cu and Cu/graphene (transferred). (A colour version of this figure can be viewed online.)

Therefore, these new nanoindentation data confirm our hypothesis that the interaction between the graphene and the substrate plays a crucial role in determining the contact behavior of graphene coated surfaces.

In conclusion, nanoindentation measurements show a significant stiffer response for Cu/graphene coated thin film than for bare Cu. This effect cannot be fully explained by the high stiffness of graphene. However, it originates from the modification of the interaction forces between the tip and the indented surface. Our results show that a single layer of CVD graphene on Cu leads thus to near ideal Hertz-like conditions by providing adhesionless (and frictionless) contact with almost no direct stiffening effect (Figs. 2a and 3b). Nanoindentation tests on graphene transferred on SiO_2 and Cu have shown opposite and weaker effects, respectively, suggesting that in order to achieve this type of adhesionless surface; the graphene-substrate interaction must be strong enough. This outstanding role of graphene in preventing material transfer could be very beneficial for various types of surface contact and MEMS applications.

Acknowledgements

The authors acknowledge financial support from the Fédération Walonie-Bruxelles through the Action de Recherche Concertée (ARC) on 3D nanoarchitecturing of 2D crystals (N° 16/21- 077). J.-J.A. and J.-C.C. acknowledges support from the Marcel De Merre Prize and from the Belgium F.R.S.-FNRS under the PDR project N° T.00014.13. Computational resources have been provided by the supercomputing facilities of the Université Catholique de Louvain (CISM/UCL) and the Consortium des Equipements de Calcul Intensif en Fédération Wallonie Bruxelles (CECI) funded by the F.R.S.-FNRS under the convention N° 2.5020.11. The authors are also grateful to Audrey Favache for the help and collaboration in this work.

Appendix A. Supplementary data

Supplementary data related to this article can be found at http://dx.doi.org/10.1016/j.carbon.2017.06.037.

References

[1] K.S. Novoselov, A.K. Geim, S.V. Morozov, D. Jiang, Y. Zhang, S.V. Dubonos, et al., Electric field effect in atomically thin carbon films, Science 306 (2004) 666–669.
[2] R. Nair, P. Blake, A. Grigorenko, K. Novoselov, T. Booth, T. Stauber, et al., Fine structure constant defines visual transparency of graphene, Science 320 (2008), 1308–1308.
[3] J.S. Bunch, S.S. Verbridge, J.S. Alden, A.M. Van Der Zande, J.M. Parpia, H.G. Craighead, et al., Impermeable atomic membranes from graphene sheets, Nano Lett. 8 (2008) 2458–2462.
[4] C. Lee, X. Wei, J.W. Kysar, J. Hone, Measurement of the elastic properties and intrinsic strength of monolayer graphene, Science 321 (2008) 385–388.
[5] S. Chen, L. Brown, M. Levendorf, W. Cai, S.-Y. Ju, J. Edgeworth, et al., Oxidation resistance of graphene- coated Cu and Cu/Ni alloy, ACS Nano 5 (2011) 1321–1327.
[6] M.-S. Won, O.V. Penkov, D.-E. Kim, Durability and degradation mechanism of graphene coatings deposited on Cu substrates under dry contact sliding, Carbon 54 (2013) 472–481.
[7] P. Goli, H. Ning, X. Li, C.Y. Lu, K.S. Novoselov, A.A. Balandin, Thermal properties of graphene-copper- graphene heterogeneous films, Nano Lett. 14 (2014) 1497–1503.
[8] S. Wang, Y. Zhang, N. Abidi, L. Cabrales, Wettability and surface free energy of graphene films, Langmuir 25 (2009) 11078–11081.
[9] K.-S. Kim, H.-J. Lee, C. Lee, S.-K. Lee, H. Jang, J.-H. Ahn, et al., Chemical vapor deposition- grown graphene: the thinnest solid lubricant, ACS Nano 5 (2011) 5107–5114.
[10] A. Klemenz, L. Pastewka, S.G. Balakrishna, A. Caron, R. Bennewitz, M. Moseler, Atomic scale mechanisms of friction reduction and wear protection by graphene, Nano Lett. 14 (2014) 7145–7152.
[11] Y. Gao, S. Kim, S. Zhou, H.-C. Chiu, D. Nélias, C. Berger, et al., Elastic coupling between layers in two- dimensional materials, Nat. Mater. 14 (2015) 714–720.
[12] J. Song, D. Srolovitz, Adhesion effects in material transfer in mechanical contacts, Acta Mater. 54 (2006) 5305–5312.
[13] D. Hyman, M. Mehregany, Contact physics of gold microcontacts for MEMS switches, IEEE Trans. Compon. Packag. Technol. 22 (1999) 357–364.
[14] H. Kwon, D.-J. Choi, J.-H. Park, H.-C. Lee, Y.-H. Park, Y.-D. Kim, et al., Contact materials and reliability for high power RF-MEMS switches, in: Micro Electro Mechanical Systems, 2007. MEMS. IEEE 20th International Conference on, 2007, pp. 231–234.
[15] B. Huet, J.-P. Raskin, Pressure-controlled chemical vapor deposition of single-layer graphene with millimeter-size domains on thin Cu film, Chem. Mater. 29 (8) (2017) 3431–3440.
[16] S. Suresh, T.-G. Nieh, B. Choi, Nano-indentation of copper thin films on silicon substrates, Scr. Mater. 41 (1999) 951–957.
[17] K.L. Johnson, K.L. Johnson, Contact Mechanics, Cambridge University Press, 1987.
[18] L. Ma, L. Levine, R. Dixson, D. Smith, D. Bahr, Effect of the spherical indenter tip assumption on the initia l plastic yield stress, in: Nanoindentation in Materials Science, InTech, 2012.
[19] H.I. Rasool, C. Ophus, W.S. Klug, A. Zettl, J.K. Gimzewski, Measurement of the intrinsic strength of crystalline and polycrystalline graphene, Nat. Commun. 4 (2013) 2811.
[20] F. Liu, P. Ming, J. Li, Ab initio calculation of ideal strength and phonon instability of graphene under tension, Phys. Rev. B 76 (2007) 064120.
[21] C. Lee, X. Wei, Q. Li, R. Carpick, J.W. Kysar, J. Hone, Elastic and frictional properties of graphene, Phys. Status Solidi B 246 (2009) 2562–2567.
[22] H. Lee, N. Lee, Y. Seo, J. Eom, S. Lee, Comparison of frictional forces on graphene and graphite, Nanotechnology 20 (2009) 325701.
[23] S. Plimpton, Fast parallel algorithms for short-range molecular dynamics, J. Comput. Phys. 117 (1995) 1–19.
[24] T.-H. Fang, C.-I. Weng, Three-dimensional molecular dynamics analysis of processing using a pin tool on the atomic scale, Nanotechnology 11 (2000) 148.
[25] L. Zhang, H. Tanaka, Towards a deeper understanding of wear and friction on the atomic scale—a molecular dynamics analysis, Wear 211 (1997) 44–53.
[26] T.-H. Fang, S.-R. Jian, D.-S. Chuu, Molecular dynamics analysis of effects of velocity and loading on the nanoindentation, Jpn. J. Appl. Phys. 41 (2002) L1328.
[27] Z. Xu, M.J. Buehler, Interface structure and mechanics between graphene and metal substrates: a first-principles study, J. Phys. Condens. Matter 22 (2010) 485301.
[28] A. Oluwajobi, X. Chen, The effect of interatomic potentials on the molecular dynamics simulation of nanometric machining, Int. J. Autom. Comput. 8 (2011) 326–332.
[29] T. Klaver, S.-E. Zhu, M. Sluiter, G. Janssen, Molecular dynamics simulation of graphene on Cu (100) and (111) surfaces, Carbon 82 (2015) 538–547.
[30] W. Wang, Q. Peng, Y. Dai, Z. Qian, S. Liu, Distinctive nanofriction of graphene coated copper foil, Comput. Mater. Sci. 117 (2016) 406–411.
[31] X. Long, B. Li, L. Wang, J. Huang, J. Zhu, S. Luo, Shock response of Cu/graphene nanolayered composites, Carbon 103 (2016) 457–463.
[32] A. Kinaci, J.B. Haskins, C. Sevik, T. Çaugin, Thermal conductivity of BN-C nanostructures, Phys. Rev. B 86 (2012) 115410.
[33] Y. Mishin, M. Mehl, D. Papaconstantopoulos, A. Voter, J. Kress, Structural stability and lattice defects in copper: Ab initio, tight-binding, and embedded-atom calculations, Phys. Rev. B 63 (2001) 224106.
[34] K. Maekawa, A. Itoh, Friction and tool wear in nano-scale machining—a molecular dynamics approach, Wear 188 (1995) 115–122.
[35] S. Li, Q. Li, R.W. Carpick, P. Gumbsch, X.Z. Liu, X. Ding, et al., The evolving quality of frictional contact with graphene, Nature 539 (2016) 541–545.
[36] Z. Deng, N.N. Klimov, S.D. Solares, T. Li, H. Xu, R.J. Cannara, Nanoscale interfacial friction and adhesion on supported versus suspended monolayer and multilayer graphene, Langmuir 29 (2012) 235–243.
[37] T. Jiang, Y. Zhu, Measuring graphene adhesion using atomic force microscopy with a microsphere tip, Nanoscale 7 (2015) 10760–10766.
[38] T. Yoon, W.C. Shin, T.Y. Kim, J.H. Mun, T.-S. Kim, B.J. Cho, Direct measurement of adhesion energy of monolayer graphene as-grown on copper and its application to renewable transfer process, Nano Lett. 12 (2012) 1448–1452.